PROCEEDINGS of the
23rd International Congress on Acoustics

9 to 13 September 2019 in Aachen, Germany

Experimental Investigation of the oscillating flow dynamics at the exit of regenerator meshes with different configurations

Islam Ramadan[1]; Helene Bailliet; Jean-Christophe Valiere

Institut Pprime, Centre National de la Recherche Scientifique, Université de Poitiers, Ecole Nationale Supérieure de Mécanique et d'Aérotechnique, Département Fluides-Thermique-Combustion, Ecole Nationale Supérieure d'Ingénieurs de Poitiers, 6 Rue Marcel Doré Bâtiment B17-BP 633, 86022 Poitiers Cedex, France

ABSTRACT

Regenerators (often consisting in stack mesh-wires) and heat exchangers are the core of thermoacoustic devices and, as such, key elements for the efficiency of these systems. In this study, the oscillating flow velocity field at the exit of different regenerators has been measured using Particle Image Velocimetry (PIV) system. Three different mesh wire sizes have been selected with respect to the size of the viscous penetration depth. The influence of the randomness of stacking the mesh wires on the oscillating flow dynamics has also been investigated. Measurements are performed for different acoustic levels. In the conference, the structure of oscillating flow will be discussed, especially in terms of vorticity fields for the different regenerators at different phases over the acoustic cycle. The evolution from low to high acoustic amplitudes will be presented.

Keywords: Thermoacoustics, End-effects, Oscillating flow, PIV

1. INTRODUCTION

The design of heat exchangers is a crucial issue for the development of efficient thermoacoustic devices. The improvement of such design requires a better understanding of flow patterns and associated heat exchange processes at the exit of the regenerator/stack. The present study aims at participating in progressing in this understanding. The synthesis of the literature on the study of oscillating flow at the exit of a thermoacoustic core is complicated by the fact that there is no agreement on the choice of the relevant dimensionless parameters. Blanc-Benon et al. [1] investigated vortex shedding from a stack of parallel plates with PIV. They studied the flow for two plate thicknesses and identified the generation of two symmetrical vortices for each plate that had different forms depending on the plate thickness. For plate thicknesses larger than the viscous penetration depth concentrated vortices were observed near the edge of the plate whereas for thinner plates elongated layers were observed without any well-defined eddies; for the range of velocity amplitudes investigated there was not any vortex street observed whatever the thickness of the plates. Mao et al. [2] compared the flow generated at the exit of a stack of plates for different plate thicknesses and found two distinct modes of generation of a vortex street: elongated shear layer on one side (observed for thin plates) and bluff-body type of shedding on the other side (observed for thick plates). They found that for high amplitudes (Reynolds numbers), vortices are shed in an alternate fashion and the Strouhal number based on the shedding velocity and acoustic amplitude is around 0.2 for all the Reynolds numbers studied. Aben et al. [3] used Strouhal and Reynolds numbers based on the plate thickness, acoustic amplitude just outside the stack, and acoustic frequency. They considered the vorticity fields for different amplitudes and different frequencies at the phase of maximum outward displacement (and zero velocity) and divided them in four categories: ''two vortices'', ''four vortices'', ''transition area'' and a ''vortex street''. One of their conclusion is that for high porosity thermoacoustic core the plate thickness is the relevant characteristic length whereas at low porosity

[1] islam.ramadan@univ-poitiers.fr

the spacing between plates is the relevant characteristic length. Shi et al. [4] used hot wire anemometry and PIV to study the flow at the exit of a stack of parallel plates for several plate thicknesses, plate spacing and Reynolds numbers (76 different flow cases). They found that only one St=f(Re) relationship was needed to correctly fit all the cases for Reynolds numbers based on plate thickness from 200 to 5000. Here the Strouhal number was defined using the vortex shedding frequency and the reference velocity was the local acoustic velocity amplitude. Then, in their study of vortex shedding at the exit of a stack of plates, Shi et al. [5] proposed to use three similarity parameters: the Reynolds number based on the plate thickness, the Keulegan–Carpenter number (KC, ratio of particle displacement amplitude to plate thickness) and lastly the Womersley number (Wo, ratio of the spacing between adjacent plates and viscous penetration depth) or equivalently the ratio of the spacing to the thickness of plates. They studied 108 different cases (different stack and amplitudes) and identified eight distinct vortex wake pattern types, among which four types have been observed and reported in previous works while the remaining four were new findings. Berson and Blanc-Benon [6] studied the flow within the gap between two stacks as a model for a stack-heat exchanger couple. They defined a Reynolds number based on the viscous boundary layer thickness and velocity amplitude inside the stack as used for the study of transition to turbulence in oscillating flow (Merkli and Thomann [7]). The Strouhal number they formed is based on the convection velocity of flow vortices and the shedding frequency. Their results showed that the Strouhal number based on the plate spacing takes values around 0.44 for all the configurations under study, whatever the Reynolds number. Also they found that at high amplitude the flow is not repeated from one acoustic period to another which involve oscillation of the cooling load viewed by the heat exchanger.

This brief bibliographic presentation shows that, even if a stack of plates is rarely used in practice, this geometry has been the most studied for what concerns end effects investigation. Flow at the exit of mesh grid regenerator, which is the most common geometry in practical devices, has never been studied to our knowledge. In the following section, the experimental setup and measurement procedure will be explained. In section 3, the results will be discussed and then the conclusions will be drawn in section 4.

2. Experimental Apparatus

2.1 Experimental setup

A schematic for the experimental setup is shown in Figure 1a. Two 8-inch loudspeakers (PHL – B2410) are mounted at both ends of the resonator which is filled with air at atmospheric conditions. The resonator is made of a square duct with inner side length of 44 mm and total length of 2645 mm. The loudspeakers are connected to a power amplifier which is driven by a function generator. They are synchronized to achieve a velocity antinode at the middle of the resonator at a resonance frequency (f) of 31 Hz. The regenerator is placed near the middle of the resonator. It consists of mesh wires stacked either randomly or forming straight channels inside a canister. The four different regenerators used in the study are shown in Figure 1b. A description of the mesh wires used in each regenerator is presented in Table 1.

In usual thermoacoustic designing tools, regenerators are described in terms of their hydraulic radius, volumetric porosity, thermal conductivity and length along the guide axis. In the present study, the mesh wire dimensions are selected to cover a plausible range for these parameters. In particular the ratio $\boldsymbol{r_o/\delta_v}$ is chosen to be credible for stack-based devices (Reg#1 and 2) or for regenerator-based devices (Reg#3 and 4). Here $\boldsymbol{r_o}$ is the hydraulic radius, which represents the ratio between the gas volume to the gas-solid contact area, and $\boldsymbol{\delta_v} = \sqrt{\nu/\pi f}$ is the viscous penetration depth where ν is the kinematic viscosity of the air. For standing-wave thermoacoustic systems, this ratio should be larger than unity and the term "stack" is used, whereas for travelling-wave system the ratio should be less than unity and the term "regenerator" is used [8].

The velocity field at one end of the regenerator is measured using PIV. The PIV system consists of a ND-YAG laser source for illuminating the seeding particles existing in the flow. An atomizer seed generator (TOPAS – ATM 210) is used to atomize oil producing droplets with mean particle diameter of 0.5 μm. Images are recorded with two 2048 × 2048 pixels^2 LAVISION cameras (maximum sampling frequency of 15 Hz). Two cameras are employed to increase the size of the measurement area without reducing the spatial resolution (i.e. 185 × 185 μm^2) of the imaging system. The PIV system is triggered by a reference external TTL signal, which is phase-locked to the acoustic

cycle.

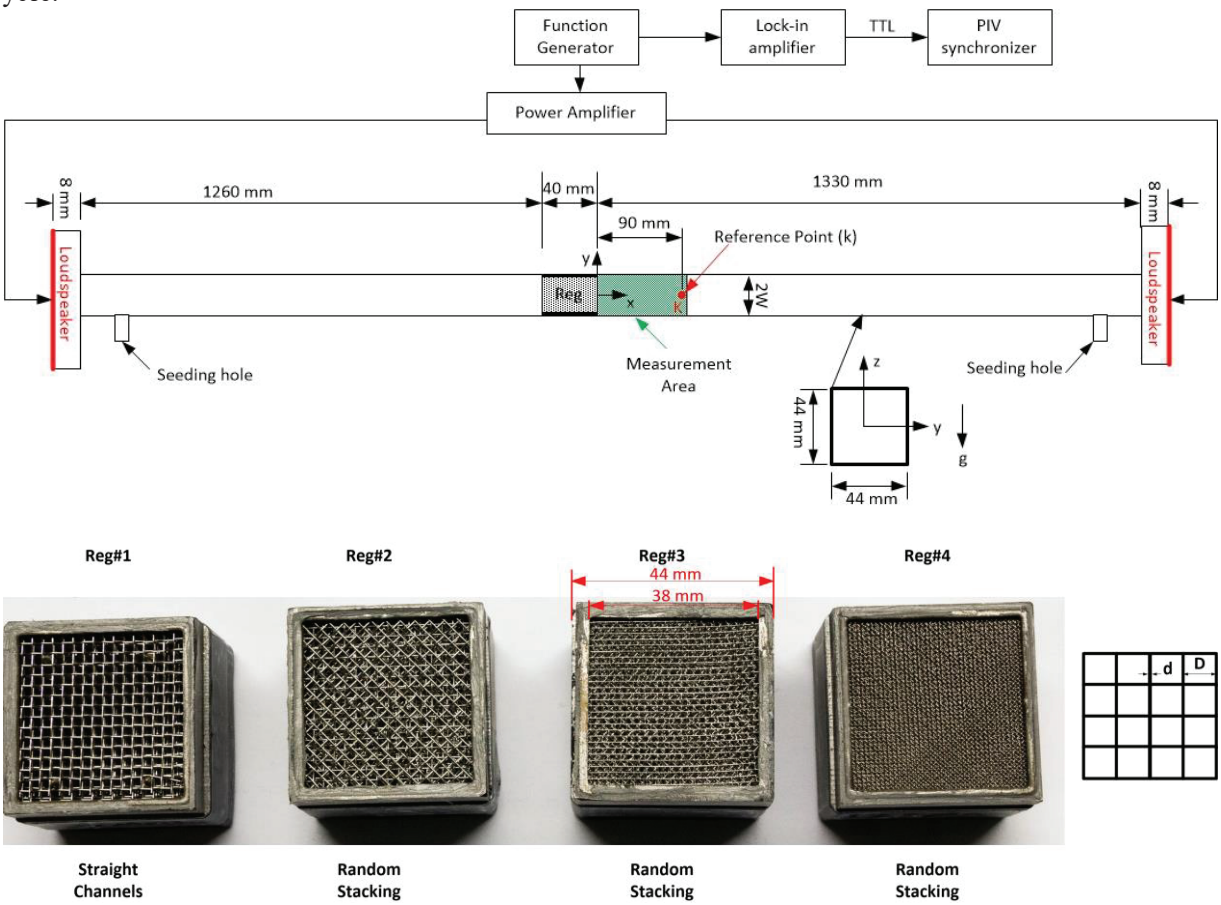

Figure 1- (a) Schematic of the experimental setup. (b) Image for the regenerators used in the study and defining parameters for the mesh wires.

Table 1: Description of the mesh wires used in each regenerator.

Name	Reg#1	Reg#2	Reg#3	Reg#4
Opening (D), mm	2.24	2.24	1.12	0.56
Wire diameter (d), mm	0.355	0.355	0.22	0.16
Volumetric porosity (%)	0.879	0.879	0.85	0.801
Hydraulic radius (r_o), mm	0.646	0.646	0.33	0.162
r_o/δ_v	1.6	1.6	0.8	0.47
Stacking configuration	Straight channels	Random	Random	Random

2.2 Experimental conditions

As mentioned previously, Aben et al. [3] used Reynolds number (Re) and Strouhal number (St)

$$Re = \frac{U_k d}{\nu}, \qquad St = \frac{fd}{U_k}$$

where U_k is the velocity amplitude at a reference point (k) (see Figure 1a) to describe the flow at the exit of a stack plates and observed three different flow patterns (i.e. two/four vortices, transition area and Vortex Street). Accordingly, the oscillating flow velocity amplitude (U_k) is adjusted so that the current experiments lay at different zones observed by [3] and hence our results can be compared with their observations. On the other hand, Shi et al. [5] found that Keulegan–Carpenter number (KC), which is defined as flows:

$$KC = \frac{X_{amp}}{d}$$

where X_{amp} is the axial displacement amplitude ($X_{amp} = \frac{U_k}{2\pi f}$), has a significant effects on the flow pattern. The experimental conditions of all the experiments, presented in Table 2, show that even if KC and St are associated with the same physics (effect of unsteadiness), in our experiments the condition for the Strouhal number is always St<<1 whereas KC goes from ≈1 to >>1.

Table 2 - The experimental conditions of different experiments

Exp#	Re	St	KC	U_k (m/s)	Reg#	Pattern ref [5]	Observed pattern
1	1.3×10^{1}	2.0×10^{-2}	8.0×10^{0}	0.56	1	2/4 vortices	shear layer
2	1.0×10^{2}	2.8×10^{-3}	5.8×10^{1}	4.0	1	Vortex street	Chaotic
3	2.3×10^{2}	1.1×10^{-3}	1.4×10^{2}	9.6	1	Vortex street	Chaotic
4	1.3×10^{1}	2.0×10^{-2}	8.0×10^{0}	0.55	2	2/4 vortices	shear layer
5	9.3×10^{1}	2.8×10^{-3}	5.7×10^{1}	3.95	2	Vortex street	Chaotic
6	2.2×10^{2}	1.2×10^{-3}	1.3×10^{2}	9.1	2	Vortex street	Chaotic
7	3.1×10^{0}	3.2×10^{-2}	4.9×10^{0}	0.21	3	2/4 vortices	no/weak vorticity
8	2.9×10^{1}	3.5×10^{-3}	4.6×10^{1}	1.95	3	Vortex street	shear layer
9	7.1×10^{1}	1.4×10^{-3}	1.1×10^{2}	4.87	3	Vortex street	Chaotic
10	2.2×10^{0}	2.4×10^{-2}	6.7×10^{0}	0.21	4	2/4 vortices	no/weak vorticity
11	1.0×10^{1}	5.1×10^{-3}	3.1×10^{1}	0.97	4	Transitional	shear layer
12	2.0×10^{1}	2.7×10^{-3}	6.0×10^{1}	1.87	4	Vortex street	shear layer

2.3 Measurement procedure and post processing

Before each experiment, the seeding holes placed at the extremities of resonator (see Figure 1a) are opened and the seeded air flow is introduced through one of these holes to create a homogenous seeding particles distribution over the measurement area. After closing the holes, the loudspeakers are turned on. The PIV measurements are started 2 minutes later, to make sure that the effect of the seeding flow on the measurements is eliminated.

As shown in Figure 2, the measurements are performed at 12 different phases over the acoustic cycle. The total number of double-images taken at each phase is 100 (this number of images were found, in previous studies [9] [10], to be sufficient for achieving the convergence of the data).

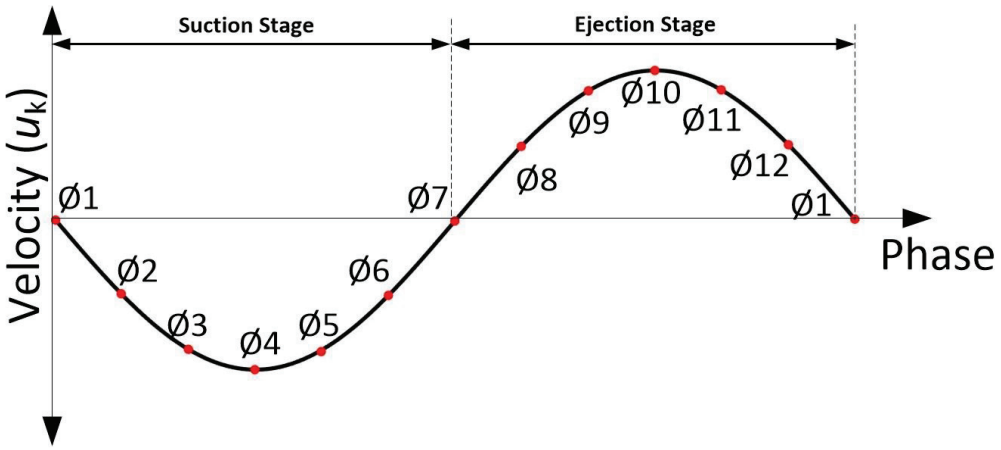

Figure 2- The acoustic velocity at different phases over the acoustic cycle at the reference point (k).

In order to produce the velocity vector maps, the acquired images are processed by DAVIS software. A low pass filter is applied to remove the light reflections from the solid walls. Then, a cross-correlation algorithm is applied to estimate the mean particles displacement within each interrogation area; finally the displacement is divided by time between two laser pulses to obtain the velocity. The time between pulses is adjusted to allow for a particle displacement equals to about ¼ the interrogation window. The ensemble-averaged vector maps and vorticity fields are calculated for each phase by averaging the 100 vector maps. In the following section, the results of the 12 experiments are discussed.

3. Results and discussions

In order to investigate the vortex patterns originated at the exit of the regenerator, the vorticity at each point in the field is calculated as follows:

$$\omega_z = \frac{dv}{dx} - \frac{du}{dy}$$

where u and v are the axial and transverse velocity components, respectively. In Figure 3 the vorticity field is plotted for all experiments at 4 phases of the acoustic cycle: $\emptyset_1, \emptyset_4, \emptyset_7$ *and* $\emptyset_{10}$ (we consider the vorticity at only 4 phases to facilitate the presentation of the results). The axial distance is normalized by the axial displacement amplitude (X_{amp}), whereas the transverse distance is normalized by the half width of the resonator (W).

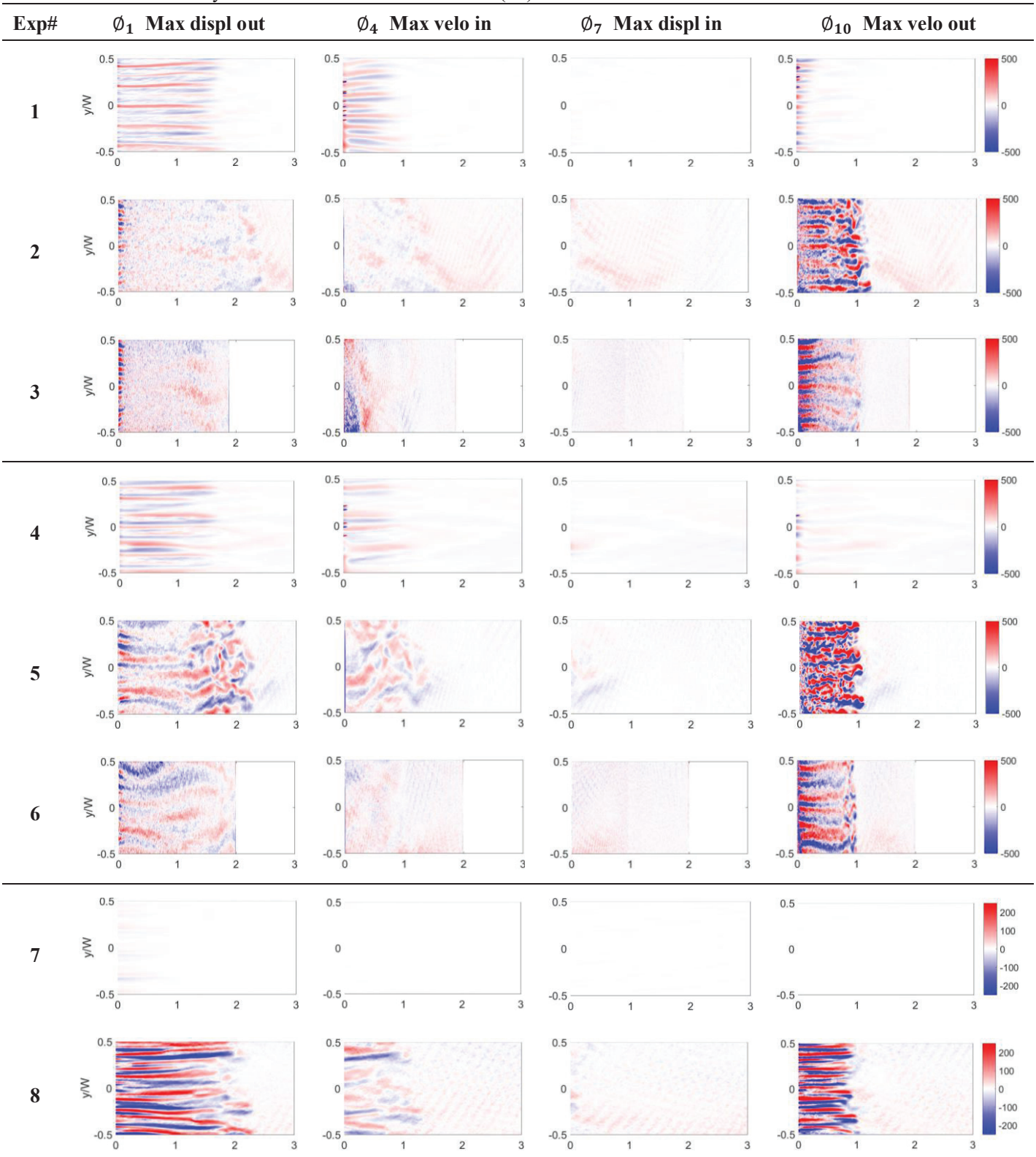

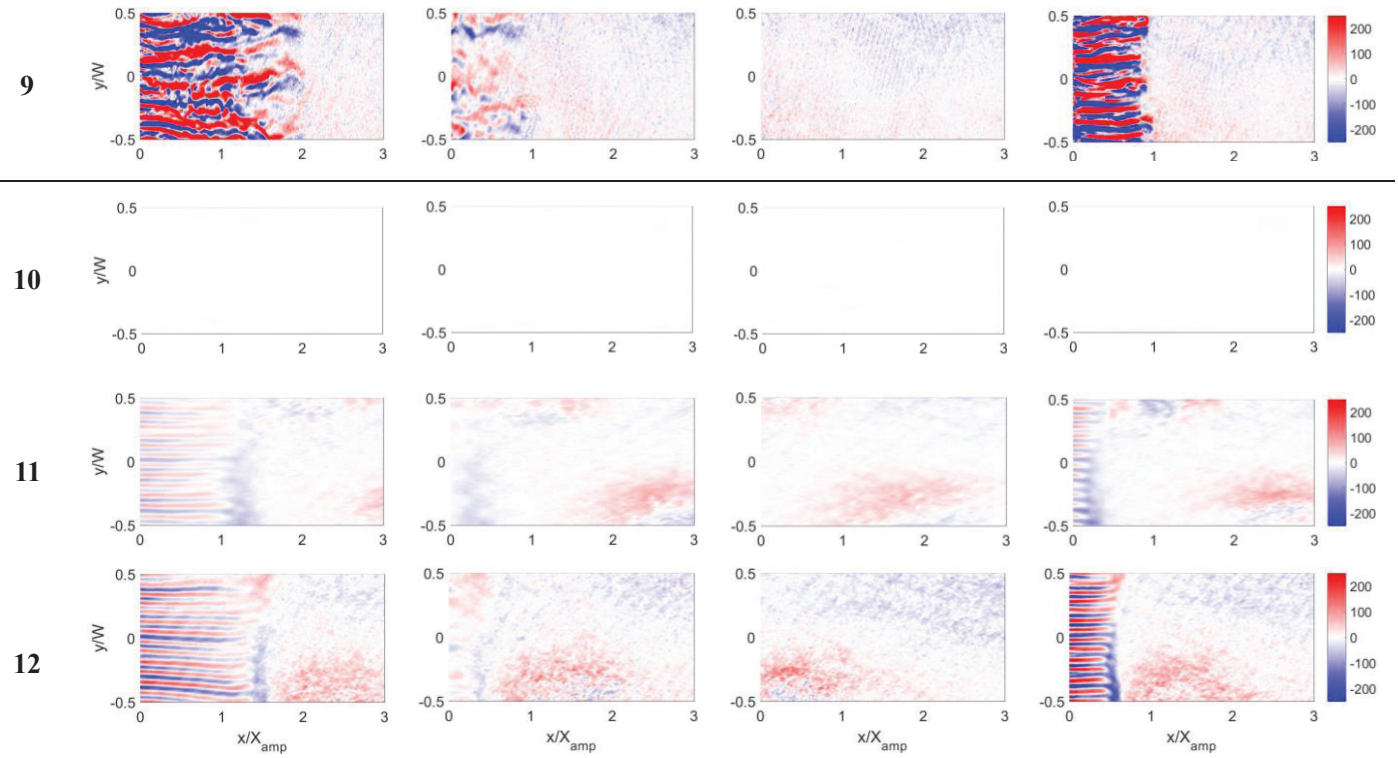

Figure 3 - The vorticity fields for all experiments at different phases over the acoustic cycle in s^{-1}.

3.1 Effects of the acoustic amplitude

As the building of more powerful thermoacoustic systems becomes a necessity, the acoustic amplitudes of these systems should be increased. However, the design of thermoacoustic systems depends mainly on the linear theory which cannot predict the non-linear phenomena especially at high acoustic amplitudes. Hence, it is important to discuss the effect of the acoustic amplitude on the oscillating flow patterns at the exit of the regenerator. For this purpose, the first three experiments are considered because the same regenerator is used but at different acoustic velocity amplitudes. As shown in Figure 3 (Exp# 1, 2 and 3), at the end of the suction stage ($\emptyset_7$), there is no vortex pattern near the exit of the regenerator because the main flow moves inwards the regenerator channels. At the beginning of the ejection stage (i.e. the flow moves outward the regenerator channels), elongated shear layers start to form and evolve till the maximum vorticity value is achieved at ($\emptyset_{10}$). At very low amplitude (Exp#1), the vorticity field at $\emptyset_{10}$ shows the emergence of alternatively opposite shear layers. These shear layers have elongated as the flow moved away from the regenerator and reach to the maximum axial normalized distance (x/X_{amp}) of 2 at $\emptyset_1$. Such vorticity layers extending out of the thermoacoustic core during ejection stage (and that prolongate the oscillating boundary layers developed inside the core) were reported by other authors for low amplitudes flow out a stack plates [6], [2]. It is also quite similar to the Elongated Symmetric vortex structures described by [5]. During the suction phase ($\emptyset_4$), the generated vortices are convected with the main flow towards the regenerator. At medium amplitude (Exp#2), the succession of elongated counter-rotating vortices is also observed. However, these elongated vortices break up at axial distance (x/X_{amp}) of 0.5 to form many rolled up vortices that extend to an axial distance (x/X_{amp}) of 1. These rolled up vortices move with the main flow while breaking up into very small structures that extend to an axial distance (x/X_{amp}) of 2.5 as shown at $\emptyset_1$. At very high amplitude (Exp#3), the flow pattern breaks down into small structures at the end of the ejection (phase $\emptyset_{10}$), that merge to form larger structures during the suction phases ($\emptyset_1$). Therefore, conversely to several previous studies [2], [6], [3] we do not observe any alternate shedding of vortices neither breaking up of the shear layers into an organized vortex street. This can be interpreted as being due to the fact that these previous studies dealt with a stack of plates whereas we are concerned with mesh grid regenerator. However, the pattern observed in the present study for high amplitude cases (Exp#2 and 3) can be classified in the "chaotic flow state and vortex merging" pattern observed by Shi et al. [5] at the exit of a stack of plates. This regime was characterized by [5] as corresponding to large KC (>>1) and Reynolds numbers (10^2 to 10^3). The

values of both Re and KC of Exp#2 and 3 fall within the range defined by [5]. As mentioned previously, the Strouhal number for all experiments is less than unity. Hence, we can consider Re and KC are the characterizing parameters for the flow patterns at the exit of the regenerator.

3.2 Effects of the stacking configuration

In order to study the effects of stacking configurations, the flow pattern at the exit of two regenerators (Reg#1 and 2) is investigated at the same flow conditions (i.e. Re, St and KC). The results of Exp#1, 2 and 3 are compared with the results of Exp#4, 5 and 6, respectively. At very low amplitude at $\emptyset_1$, it is observed that the flow pattern in the case of random stacking (i.e. Exp#4) is less organized than in the case with straight channels (i.e. Exp#1); in particular the repeatability in the vertical direction observed for the straight channel is not as marked in the random stacking case. At medium amplitude at $\emptyset_{10}$, the beak up of the flow in numerous small structures occurs for a shorter distance from the regenerator end in the case of random stacking (i.e. Exp#5) than in the case of straight channels (i.e. Exp#2). At very high amplitude, the stacking configuration seems to have no much influence on the flow pattern (comparing Exp#3 and 6).

3.3 Effects of the mesh-wire size

To investigate the effects of the mesh-wire size on the flow pattern, the flow pattern at the exit of 3 different regenerators (Reg#2, 3 and 4) is investigated at different experimental conditions. The flow conditions are adjusted so that KC number has the same order of magnitude at different mesh-wire sizes. For instance, the KC number of Exp# 4, 7 and 10 has the same order of magnitude whereas the mesh-wire size in these three experiments is different. For this purpose, the results of Exp#4, 5 and 6 are compared with either Exp#7, 8 and 9 or Exp#10 and 11/12, respectively. It is worthwhile to mention that the intensity of the vorticity field has been reduced in the cases of Reg#3 and 4. Hence, the scale of the vorticity in Exp#7 to 12 has been reduced by half (+/-250 instead of +/-500) to make the flow patterns visible.

As shown in Figure 3, at very low velocity amplitudes (Exp#4, 7 and 10), the decrease of the mesh-wire size results into a decrease in the intensity of the vorticity field. According to the observations of [3] in the case of parallel-plates stack, the flow pattern in these three experiments (Exp#4, 7 and 10) should be similar. In the current study, we observed that the flow pattern is different from the observations of [3] in the case of large mesh-wire size (Exp#4). With smaller mesh-wires size (Exp#7 and 10), the vorticity is negligible over the whole cycle. At medium flow velocity amplitudes (Exp#5, 8 and 11), it is observed that (see $\emptyset_1$) the elongated vortices break up into smaller vortices with large mesh-wire size (Exp#5) whereas the breakup of the elongated vortices was not observed with smaller mesh-wire size (Exp#8 and 11). At high flow velocity amplitudes (Exp#6, 9 and 12), it is observed that (see $\emptyset_1$) the elongated vortices beak up with the cases of large and medium mesh-wire sizes (Exp#6 and 9) whereas there is no breakup observed with the case of small mesh-wire size. As was concluded from section 3.1, it appears then that the flow classification and similarity parameters chosen by Aben et al. [3] for their study of end effects for a stack of plates do not correspond to the observation made in our study.

4. CONCLUSION

In the current study, the oscillating flow patterns at the exit of different regenerators have been investigated. Three main flow patterns were observed namely; no/weak vorticity pattern, shear layer pattern and chaotic pattern. The effects of different parameters on the flow patterns have been investigated. First, the effects of the flow velocity amplitude have been investigated. We found that both Re and KC are well suited similarity parameters for the flow pattern at the exit of the regenerator. Second, the effects of the stacking configuration of the mesh-wires in the regenerator have been investigated. The random stacking of the mesh-wires altered the flow patterns at low and medium velocity amplitudes whereas the flow pattern does not changed at higher velocity amplitudes. Finally, the effects of the mesh-wire size on the flow pattern have been investigated. Reducing the mesh-wire size results in decreasing the intensity of the vorticity, which confirm the validity of the Reynolds number as similarity parameter.

ACKNOWLEDGEMENTS

This research is financially supported by Agence Nationale de la Recherche (Projet-ANR-17-CE06-0007-

01). The authors also appreciate the technical assistance provided by Pascal Biais, Laurent Philippon and Philippe Szeger.

REFERENCES

1. Blanc-Benon P, Besnoin E, Knio O. Experimental and computational visualization of the flow field in a thermoacoustic stack. C R Mec. 2003;331:17–24.
2. Mao X, Yu Z, Jaworski A, Marx D. PIV studies of coherent structures generated at the end of a stack of parallel plates in a standing wave acoustic field. Exp in Fluids. 2008;45:833–846.
3. Aben P, Bloemen P, Zeegers J. 2-D PIV measurements of oscillatory flow around parallel plates. Exp Fluids. 2009;46:631–41.
4. Shi, L, YU Z, Jaworski A. Investigation into the Strouhal numbers associated with vortex shedding from parallel-plate thermoacoustic stacks in oscillatory flow conditions. European Journal of Mechanics B/Fluids. 2011;30:206–17.
5. Shi, L, YU Z, Jaworski A. Vortex shedding flow patterns and their transitions in oscillatory flows past parallel-plate thermoacoustic stacks. Experimental Thermal and Fluid Science. 2010;34:954–65.
6. Berson A, Blanc-Benon P. Nonperiodicity of the flow within the gap of a thermoacoustic couple at high amplitudes. J Acoust Soc Am. 2007;122(4).
7. Merkli P, Thomann H. Transition to turbulence in oscillating pipe flow. J Fluid Mech. 1975;68:567–575.
8. Swift G. Thermoacoustics: a unifying perspective for some engines and refrigerators. Acoustical Society of America; 2002.
9. Mao X, Jaworski A. Application of particle image velocimetry measurement techniques to study turbulence characteristics of oscillatory flows around parallel-plate structures in thermoacoustic devices. Meas Sci Technol. 2010;21.
10. Ramadan I. Experimental Investigation of Non-linearities in Thermoacoustic Systems: Streaming, Transition to Turbulence and Entrance Effects. The American University in Cairo; 2018.